# **Soft Matter**



PAPER View Article Online
View Journal | View Issue



**Cite this:** *Soft Matter,* 2019, **15**. 8800

Received 6th August 2019, Accepted 3rd October 2019

DOI: 10.1039/c9sm01579e

rsc.li/soft-matter-journal

# The influence of fractional surface coverage on the core-core separation in ordered monolayers of thiol-ligated Au nanoparticles

Morgan Reik,<sup>a</sup> Melanie Calabro,<sup>a</sup> Sean Griesemer, <sup>D</sup> Edward Barry,<sup>b</sup> Wei Bu, <sup>D</sup> Binhua Lin <sup>D</sup> \*<sup>ac</sup> and Stuart A. Rice <sup>D</sup> \*<sup>a</sup>

We report the results of grazing incidence X-ray diffraction (GIXD) measurements from water supported Langmuir monolayers of gold nanoparticles ligated with dodecanethiol (12 carbons), tetradecanethiol (14 carbons), hexadecanethiol (16 carbons), and octadecanethiol (18 carbons). These monolayers are formed from solutions with varying concentrations of the respective thiols. We show that equilibrium between adsorbed thiol molecules and the thiols in the bulk solution implies fractional coverage of the Au nanoparticle core. We also show that the nanoparticle–nanoparticle separation and the correlation length of particles in these ordered films increases with thiol concentration in the parent solution, and that excess thiol can be found in the space between particles as well as in islands away from the particles. Using the equilibrium constant relating ligand solution concentration and nanoparticle surface coverage of the gold core by the ligand molecules, we interpret the way in which varying thiol concentration affects the nanoparticle–nanoparticle separation as a function of surface coverage of the gold core by the ligand molecules.

### Introduction

Metal nanoparticles are microcrystalline aggregates of a few thousand metal atoms, a few nanometers in diameter, frequently modified with organic capping ligands to which they are chemically bonded. The properties of such ligated nanoparticles have been the subject of many studies over the last several decades due to their novel optical<sup>1-3</sup> and electronic<sup>4-6</sup> properties and the ease with which they self-assemble into long-range ordered two-dimensional (2D) films when deposited on a liquid or solid surface.<sup>7-9</sup> These features lead to numerous applications of nanoparticle films in a wide range of fields ranging from nanotechnology<sup>10-12</sup> to biology.<sup>13-16</sup> Further development of these applications requires a deep understanding of how and by what forces the nanoparticle structure of a film is determined, and of methods with which the film structure can be tuned so as to embody specific properties for particular scientific applications.

The ligands that dress a metal nanoparticle play a crucial role in determining the properties of the ligated particle films, because the ligand–ligand interactions are mainly responsible for the nature of the interparticle interactions in the film. Several studies of the influence of ligand length<sup>17–20</sup> and

composition<sup>9,21–23</sup> on the nanoparticle–nanoparticle pair interaction and on the properties of nanoparticle films have been reported, but we have only partial understanding of the molecular and structural origins of these properties; a review of the current interpretation of the role of soft ligands in determining nanoparticle superlattice structure is presented in ref. 24. However, the issue of particular interest to us, which is the variation of film properties with the fractional coverage of the nanoparticle surface, is incompletely examined.

It is commonly assumed, without presentation of verification, that the nanoparticle surface is maximally covered with ligands. Maximum packing density for alkanethiols adsorbed to a flat Au(111) surface is about 4.6 alkanethiols per nm<sup>2</sup> (corresponding to an area per molecule of 21.6 Å<sup>2</sup> per alkanethiol<sup>25,26</sup>); here, we assume that this value is the same for our Au spheres, as it is conventional to do so for alkanethiol binding to Au cores with diameters larger than about 4 nm.<sup>27</sup> Using this value, we can conclude from reviewing studies of adsorption of various thiols to Au that surface coverage remains below the maximum amount of 4.6 thiols per nm<sup>2</sup>, even for thiol concentrations considered relatively high in experimental settings, as the free energy of binding of an alkanethiol to the Au core is not so large that its surface is always fully covered with ligands according to these studies. Put another way, we expect the fractional coverage of the surface of the Au core by thiol ligands to vary with variation of the thiol concentration in the solution used in the preparation.

<sup>&</sup>lt;sup>a</sup> James Franck Institute, University of Chicago, Chicago, IL 60637, USA. E-mail: lin@cars.uchicago.edu, sarice@uchicago.edu

<sup>&</sup>lt;sup>b</sup> Applied Materials Division, Argonne National Laboratory, Argonne, IL 60439, USA

<sup>&</sup>lt;sup>c</sup> NSF's ChemMatCARS, University of Chicago, Chicago, IL 60637, USA

Paper

We utilize previous studies of thiol adsorption on Au to estimate the way in which ligands coat the surface of our NP samples; 28-32 however, we note that studies of thiol binding to a flat microcrystalline film of gold, or to a gold nanoparticle, are subject to a number of experimental difficulties, amongst which the cleanliness of the surface and the heterogeneity of the surface are prominent. Small Au cores, say with linear dimensions of the order of 1 nm, are faceted crystals that expose several crystal planes and edges that have different affinities for the SH group of the thiol ligand. Large Au cores, say with linear dimensions of the order of 5 nm, are nearly spherical with many small area facets, hence statistically almost homogeneous and can be plausibly modelled to have a uniform affinity for the SH group of the thiol ligand. As with all studies of surface chemistry, the cleanliness of the surface plays a large role in the processes that occur. Studies of the adsorption of thiols on flat Au films rarely report verification of the existence of a clean surface, and studies of thiol adsorption to Au nanoparticles must contend with the preparation scheme, which often employs conditions that utilize capping molecules to protect the core surface. In the latter case the adsorption of the thiol molecule on the core surface must be an exchange reaction that may have a complex mechanism. It is not surprising that reports of the kinetics of thiol adsorption on Au, while displaying overall qualitative agreement, differ somewhat from one another.<sup>28–32</sup>

We employ Langmuir kinetic models to determine the equilibrium fractional surface coverage of our thiol-coated Au-NP systems; comparable studies by Karpovich and Blanchard<sup>31</sup> as well as Durning and Turro28 demonstrate that alkanethiols binding to gold are described by Langmuir kinetics, but there are notable differences between these studies. Karpovich and Blanchard's study, which uses quartz crystal gravimetry to study dodecanethiol binding to a flat surface of gold, reports that adsorption is well described by Langmuir kinetics; the Langmuir kinetics fit to their data implies that full coverage corresponds to a monolayer of ligands. The secondary implication of that fit is, obviously, that the equilibrium fractional surface coverage depends on the concentration of dodecanethiol to which the surface is exposed. The study by Durning and Turro, using the same technique, reports that although the gross aspects of the adsorption kinetics follow the Langmuir model there are two important deviations from that model: the equilibrium (asymptotic) coverage of the surface is greater than a monolayer, specifically about 1.2 monolayers, and the character of the deviation of the data from the Langmuir model fit suggests that the adsorption is a two-stage process, fast in the early stage and slow in the later stage. That the adsorption of thiols on Au is a two-stage process was first hinted at in an earlier study reported by Bain et al. 18 Another uncertainty in the data in the literature is the time scale for the adsorption process, which differs considerably in the several reports. <sup>28,31,33</sup> These differences in time scale are attributed to variations in the conditions used in the solution deposition process (e.g. stirring vs. no stirring), to different choices of solvent for the thiol and to different surface contaminations. However, the two-stage nature of the adsorption mechanism is supported by the majority of the studies and the accuracy of the description of the second stage with Langmuir kinetics has

been cleanly verified by the work of Cheng et al.34 in a study of dodecanethiol adsorption to AuNPs.

Understanding the nature of the adsorption process offers additional insight into the morphological behavior of Langmuir monolayers; Griesemer et al.35 have shown that the mechanical properties of Au-ligated nanoparticle films supported at the air-water interface are greatly influenced by the ligand concentration, specifically by a marked reduction of the compressive and shear moduli as the ligand concentration increases. TEM images of films derived from these monolayers reveal that increasing the ligand concentration results in a greater NP-NP separation and the nucleation of clusters of excess ligands. They also show that increasing the ligand concentration results in a shift in the monolayer collapse mode from wrinkling and folding at low concentrations to multilayer formation and subsequent wrinkling and folding at higher concentrations, with the change in monolayer morphology accompanied by decreasing pressure during monolayer and buckling stages. Although these changes in morphology and mechanical properties obviously are generated by changes in the ligand mediated NP-NP interactions the experiments do not distinguish between the roles played by change in ligand fractional coverage, change in ligand-ligand interpenetration and the distribution of excess ligand molecules. We report, in the following, grazing incidence X-ray diffraction (GIXD) measurements from water supported films of AuNPs ligated with dodecanethiol, tetradecanethiol, hexadecanethiol, and octadecanethiol. The water supported Langmuir monolayers are formed from solutions with different concentrations of the respective thiols, which enables us to examine the way in which varying thiol concentration affects the NP-NP separation.

To interpret our experimental data, we must determine how the fractional coverage of the AuNP core depends on the thiol concentration. A qualitative analysis of the dependence of AuNP surface coverage on the thiol concentration in a monolayer can be developed despite the uncertainties in the adsorption studies described above. We have opted to use the free energies of adsorption reported by Karpovich and Blanchard,31 as well as Ansar et al., 32 to estimate, for the systems studied in this paper, the free energies of adsorption and thereby the fractional nanoparticle surface coverage as a function of thiol concentration in solution. Our findings demonstrate that the NP-NP separation and correlation length of particles in these films increases linearly with thiol concentration in the parent solution, indicating that the bulk thiol is in equilibrium with the thiol on the core surface, and that excess thiol can be found in the space between particles.

# Experimental details

### A. Nanoparticle samples

The AuNP samples ligated with dodecanethiol (12 carbons) in these studies were the same as used by Griesemer et al.35 "Batch 1" was purchased from Ocean Nanotech (Lot #081715); these NPs have a core diameter of 5.4  $\pm$  0.1 nm. "Batch 2" was synthesized

Soft Matter

using a digestive ripening technique;<sup>36</sup> these NPs also have a core diameter of 5.4  $\pm$  0.1 nm. The samples of Au particles ligated with tetradecanethiol (14 carbons), hexadecanethiol (16 carbons), and octadecanethiol (18 carbons) used in these studies were synthesized using the same digestive ripening technique as for the dodecanethiol ligated Au particles; these NPs had core diameters of 5.2  $\pm$  0.1 nm, 6.6  $\pm$  0.1 nm, and 6.7  $\pm$  0.1 nm respectively. The Au core diameters quoted were determined from fits of the respective GIXD pattern to the form factor of a sphere (see Experimental results and discussion section for details).

Prior to use to prepare Langmuir monolayers for GIXD studies, the AuNP samples were washed extensively (three to four times) with ethanol to reduce the concentration of the unbound ligands and any remaining reaction agent in the solution, then centrifuged to separate the AuNPs from the supernatant liquid (see Supplementary information in ref. 37 for detailed procedure). The S and Au concentrations in the extensively washed AuNP preparations were determined by inductively coupled plasma-optical emission spectroscopy (ICP-OES) using an Agilent 700 Series spectrometer to determine the initial Au and thiol concentrations. A sample for ICP-OES analysis was prepared by drying the centrifugate, then completely dissolving it in a mixture of aqua regia and deionized water. The concentration of AuNPs in all extensively washed samples is 1 mg mL<sup>-1</sup> (about  $7 \times 10^{14}$  AuNPs per mL), and the solvent was toluene in each case. Specific amounts of thiols were then added to the washed samples to generate AuNPs of different thiol concentrations in solution, resulting in different surface coverages of thiols on Au cores, which were used to prepare Langmuir monolayers for GIXD studies.

#### B. Estimated AuNP fractional surface coverage by ligands

As we have noted above, there is considerable uncertainty in the results obtained from the several studies of the kinetics of thiol adsorption to Au. Nevertheless, we argue that a qualitative analysis of the dependence of AuNP surface coverage on the thiol concentration in a monolayer can be developed from those data, and that said analysis is useful in the interpretation of the thiol concentration dependence of the GIXD data. We assume that the characterization of the second stage of the kinetics of adsorption by the Langmuir adsorption model is sufficiently accurate that the thiol concentration in solution, C, and the time dependent surface coverage,  $\theta(t)$ , can be represented in the form

$$\theta(t) = \frac{C}{C + \left(\frac{k_d}{k_a}\right)} [1 - \exp(-(k_a C + k_d)t)], \tag{1}$$

with  $k_a$  and  $k_d$  the rate constants for adsorption and desorption, respectively, and  $K_{\rm eq} = k_{\rm a}/k_{\rm d}$  the equilibrium constant for adsorption.31 Then, the fractional surface coverage of the Au core by ligands when equilibrium with the bulk solution is established has the simple form

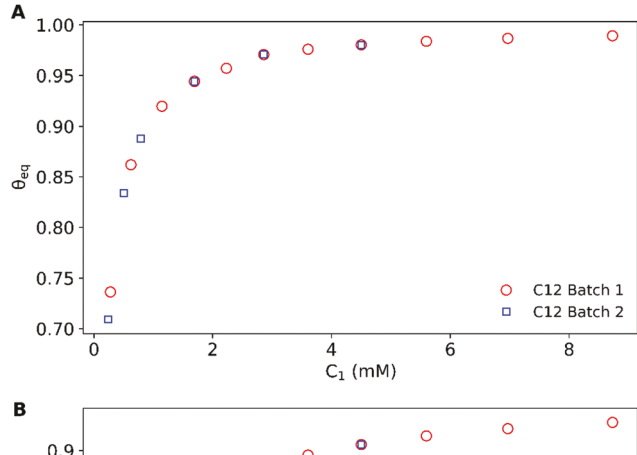
$$\theta_{\rm eq} = \frac{C}{C + \left(\frac{1}{K_{\rm eq}}\right)}.$$
 (2)

Values of the adsorption equilibrium constants have been reported for three systems similar to ours. These are octane thiol binding to a microcrystalline flat gold surface in hexane and toluene,31 octadecane thiol binding to a microcrystalline flat gold surface in hexane and toluene,31 and dodecane thiol binding to gold nanoparticles in toluene.<sup>32</sup> The free energies of adsorption of a particular thiol,  $\Delta G_{ads} = -RT \ln K_{eq}$ , are not overly sensitive to the solvent provided that solvent is not miscible with water. For example, the free energies of adsorption of dodecane thiol onto a flat microcrystalline gold surface from hexane and similarly from cyclohexane are  $-23.4 \pm$ 0.8 kJ per mole and  $-23.0 \pm 1.7$  kJ per mole, respectively.<sup>31</sup> Therefore, we assume it is valid to use the equilibrium constants obtained for adsorption from hexane to make predictions about the equilibrium constants for adsorption from toluene. Studies of the heats of desorption from Au of linear alkanes and alkane thiols are known to be linear in the number of carbons in the chain and we assume that the equilibrium constant of adsorption will likewise be linear in the number of carbons in the ligand chain. As a result, the equilibrium constants for the adsorption of tetradecanethiol and hexadecanethiol on AuNP can be determined through a linear fit of the three equilibrium constants found in the references. A least-squares linear fit to the equilibrium constants of adsorption for the three systems identified above<sup>31,32</sup> leads to  $K_{eq} = 1296n - 7355$ , with *n* being the number of carbons in the ligand chain. Reference and fitted values of  $K_{\rm eq}$  and  $\Delta G_{\rm ads}$  for alkane thiols with  $8 \le n \le 18$  are displayed in Table 1. As indicated above,  $\Delta G_{ads}$  for the samples used in this work is not large, and, therefore, fractional surface coverage of alkanethiols is expected to accompany variation of the thiol concentration in solution. With the values of the adsorption equilibrium constants we are able to calculate the fractional surface coverage of the AuNP as a function of bulk thiol concentration.

The ICP-OES analysis yields the mass of Au and the sum of the masses of S in the solution as free thiol and adsorbed to the Au cores; the former sum must be parsed into its contributions to calculate the surface overage of the AuNP. This is particularly important when calculating the surface coverage of AuNPs of extensively washed AuNP solutions in which the mass of the thiols in the solution is comparable to that adsorbed to the Au cores (Fig. 1B). If  $N_{\text{sat}}$  is the maximum number of thiols that can adsorb on the Au cores (corresponding to 4.6 thiols per nm<sup>2</sup>),  $N_1$  and  $N_2$  the numbers of thiol molecules in solution and

 $\textbf{Table 1} \quad \textbf{Reference and fitted equilibrium constants, } \textit{K}_{\text{eq}}, \text{ and free energies}$ of adsorption,  $\Delta G_{ads}$ , of several alkanethiols to Au

| $n_{ m thiol}$ | Reference $K_{\rm eq} (M^{-1})$ | Fitted $K_{\rm eq} \left( \mathbf{M}^{-1} \right)$ | Reference $\Delta G_{\rm ads}$ (kJ mol <sup>-1</sup> ) | Fitted $\Delta G_{\rm ads}$ (kJ mol <sup>-1</sup> ) |
|----------------|---------------------------------|--|--|---|
| 8              | $1.93 	imes 10^3 \pm$           | _  | -18.4  | _   |
|                | $8.4 \times 10^2$               |  |  |   |
| 12             | $1.00\times10^4$                | _  | -22.4  | _   |
| 14             | _                               | $1.08 	imes 10^4$                                  | _  | -22.6   |
| 16             | _                               | $1.34 \times 10^{4}$                               | _  | -23.1   |
| 18             | $1.53\times10^4~\pm$            | _  | -23.5  | _   |
|                | $7.3 \times 10^{3}$             |  |  |   |



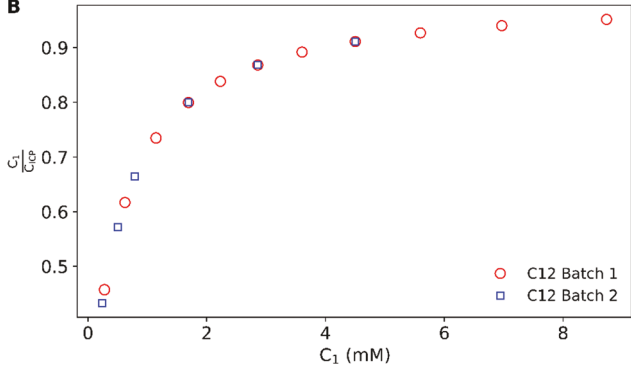


Fig. 1 (A) The calculated fractional surface coverage of the AuNP as a function of thiol concentration in solution,  $C_1$ , for dodecane thiol ligated nanoparticles, using eqn (3). (B) The ratio of  $C_1/C_{\rm ICP}$  as a function of  $C_1$  for dodecane thiol ligated nanoparticles, where  $C_{\rm ICP}$ , determined using ICPOES, is the sum of the thiols in solution,  $C_1$ , and that adsorbed on Au cores,  $C_2$ . Data points represent thiol concentrations which were used for the GIXD measurements in this work.

adsorbed on the Au cores, respectively,  $N_{\rm ICP}$  the total numbers of thiol molecules in the sample, then,  $N_{\rm ICP} = N_1 + N_2$ ,  $\theta_{\rm eq} = N_2/N_{\rm sat}$ , and  $N_1 = N_{\rm ICP} - N_2 = N_{\rm ICP} - N_{\rm sat}\theta_{\rm eq}$ . Converting N to concentration of thiols, C, we have  $C_{\rm ICP} = C_1 + C_2$ ,  $\theta_{\rm eq} = C_2/C_{\rm sat}$ , and  $C_1 = C_{\rm ICP} - C_2 = C_{\rm ICP} - C_{\rm sat}\theta_{\rm eq} = C_{\rm ICP} - C_{\rm sat}C_1[C_1+(1/K_{\rm eq})]^{-1}$ , which results in a quadratic function for the bulk thiol concentration,  $C_1$ ,

$$C_1^2 + \left(C_{\text{sat}} - C_{\text{ICP}} + \frac{1}{K_{\text{eq}}}\right)C_1 - \left[\left(\frac{1}{K_{\text{eq}}}\right)(C_{\text{ICP}})\right] = 0.$$
 (3)

With the value of the equilibrium constants given in Table 1 and  $C_{\rm ICP}$  from the ICP-OES analysis, this equation can be solved for  $C_1$ , and noting that  $C_1 = C$  in Eqn (2), we can calculate  $\theta_{\rm eq}$ . The dependence of  $\theta_{\rm eq}$  and  $C_1/C_{\rm ICP}$  on  $C_1$  is displayed in Fig. 1A and B, respectively, for all the AuNP samples used for this work.

We find that at the bulk thiol concentration used in most experiments the Au cores are not fully covered with ligands. Indeed, it takes a much greater concentration of thiol than commonly used in the AuNP solution to generate within 1% of full coverage, hence the assumption that the Au nanoparticle cores are always fully covered at any bulk thiol concentration is not valid. It follows that increasing the thiol concentration of a solution of AuNPs that then is used to form a self-assembled

monolayer or other structure is likely to lead to a thiol dependence of the NP-NP separation and, at sufficiently high thiol concentration, to formation of islands of excess thiol.

# C. Nanoparticle film preparation, GIXD measurements and TEM imaging

GIXD scattering experiments were performed at NSF's Chem-MatCARS 15-ID beamline at the Advanced Photon Source, Argonne National Laboratory. A schematic of liquid surface X-ray scattering measurements for an AuNP film on the surface of water is shown in the TOC, and details of the experimental setup can be found elsewhere. <sup>38,39</sup> Briefly, a monochromatic X-ray beam of wavelength  $\lambda$  = 1.24 Å is directed onto the air-water interface (defined by the *x*-*y* plane) at a grazing incident angle ( $\alpha$ ). Two-dimensional (2D) GIXD patterns are measured along the interface ( $\theta$ ) in a range of out-plane angles ( $\beta$ ), and plotted in the  $Q_{xy}-Q_z$  plane, where  $Q_{xy}=2k\sin(\theta/2)$ ,  $Q_z=k(\sin\alpha+\sin\beta)$ , and  $k=2\pi/\lambda$ .

Monolayer films of AuNPs were prepared on a custom-made Langmuir trough. All trough experiments were conducted at 20 °C. The trough was first cleaned with chloroform and then filled with de-ionized water. A mechanical barrier that confines the air-water interface can freely move along the *x*-axis of the trough and vary the trough area with the width of the trough fixed. A NIMA balance at the fixed end of the trough holds a paper  $2 \times 1 \text{ cm}^2$  Wilhelmy plate pressure sensor oriented parallel to the barrier. To ensure cleanliness of the water surface a test run is performed by compressing the barrier while the pressure is maintained below 0.1 mN m<sup>-1</sup>.

A sample of AuNPs is slowly deposited on the surface of the water by touching a drop of solution from the tip of a syringe. After allowing the solvent to evaporate for a few seconds, another droplet is deposited, and the process is repeated until the trough appears to be evenly filled with the dark-purple particles. The surface pressure at this point is typically around 1 mN m<sup>-1</sup>. It is important to note that the vapor pressures of the thiols we have used are sufficiently low that the unbound thiol in the AuNP suspension in toluene does not evaporate when a drop of the suspension is deposited on the water surface of the Langmuir trough; only the toluene evaporates. After deposition, the trough is sealed and flushed under helium for 15 minutes, and the sample is then compressed by the trough barrier at a rate of 5 cm<sup>2</sup> min<sup>-1</sup> until the surface pressure reaches at 5 mN m<sup>-1</sup>. GIXD measurements were performed at a constant trough area, and the surface pressure was essentially constant throughout the measurements.

It has been reported that, upon spreading onto the surface of water, AuNPs self-assemble into a close-packed 2D crystalline monolayer, and that the monolayer buckles into multilayers at a surface pressure higher than about 8–10 mN m $^{-1}$ . $^{35,38,39}$  The isotherms of monolayers of fully compressed AuNPs from batches 1 and 2 were reported by Griesemer *et al.* $^{35}$  In addition, these studies have shown that the spacing between AuNPs, determined using GIXD, does not depend on the surface pressure.

Soft Matter

For TEM studies, monolayers of AuNPs were transferred, by the Langmuir-Schaefer deposition method, to a 15 nm silicon nitride substrate over a 200 mm silicon wafer with a  $0.25 \times 0.25 \text{ mm}^2$ window (Ted Pella) for TEM imaging (see ref. 35 for details).

# Experimental results and discussion

Fig. 2A shows a typical 2D GIXD pattern for a monolayer of dodecanethiol ligated AuNPs at the air-water interface. As reported previously,<sup>39</sup> the diffraction pattern shows truncationrod type of Bragg peaks of a hexagonal ordering to the 5th order, indicating that the AuNP films form well-ordered 2D hexagonally packed crystal domains at the interface. The center-to-center NP-NP separation,  $D_{C-C}$ , can be determined from the Bragg peaks to within 1 Å. The white lines on the plot trace the minima of the form factor from the diffraction of the Au cores, which can be used to determine the average size of the Au cores,  $D_{\text{core}}$ , to within 1 Å. Fig. 2B shows 1D GIXD data (integrated over  $Q_z$ ) for monolayers of dodecanethiol ligated

0.3 0.1 0.05 0.10 0.20 0.25 0.30  $Q_{xy} \ [\mathring{A}^{-1}]$ B 0.28 mM 101 1.69 mM 6.97 mM 100

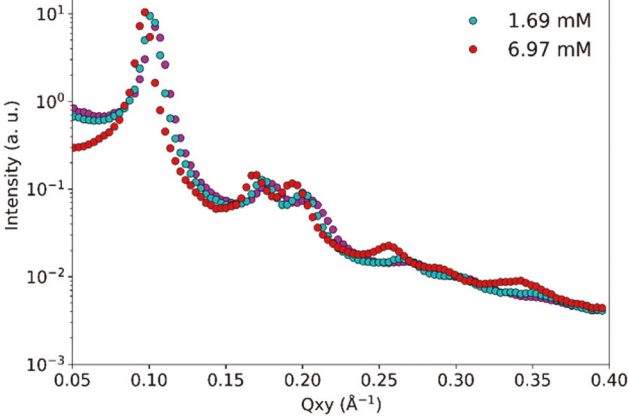
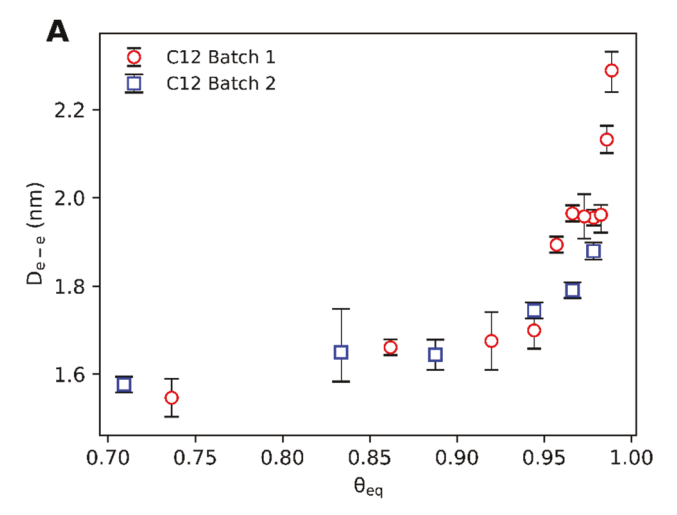


Fig. 2 (A) Typical 2D GIXD pattern for a monolayer of dodecanethiol ligated AuNPs at the air-water interface. (B) GIXD data integrated over  $Q_z$  for dodecane thiol ligated AuNP monolayers with different bulk thiol concentrations

AuNPs from sample batch 2 with different thiol concentrations in the monolayers.

It is apparent from Fig. 2B that both the Bragg peak positions and the width of the peaks change as the thiol concentration changes, indicating that both the AuNP particle separation,  $D_{C-C}$ , and the domain size of the AuNPs (which are inversely proportional to the width of the diffraction peak) change as the thiol concentration changes. As show in Fig. 1, change of thiol concentration in the AuNP solution,  $C_1$ , leads to change in the surface coverage of the thiols on the Au cores,  $\theta_{\rm eq}$ , as dictated by the equilibrium constant. Therefore, we plot the GIXD results as a function of the surface coverage,  $\theta_{eq}$ .

Fig. 3A shows the edge-to-edge NP-NP separation,  $D_{\rm e-e}$  ( $D_{\rm e-e} = D_{\rm c-c} - D_{\rm core}$ ), as a function of  $\theta_{\rm eq}$  for dodecanethiol ligated AuNPs (for batch #1 and batch #2), and the error bar was determined from repeated GIXD measurements on each monolayer (the schematic for  $D_{e-e}$  is illustrated in the TOC figure). As the surface coverage is increased,  $D_{e-e}$  increases at a similar rate for both batches of AuNPs. Fig. 3B shows  $D_{e-e}$  as a



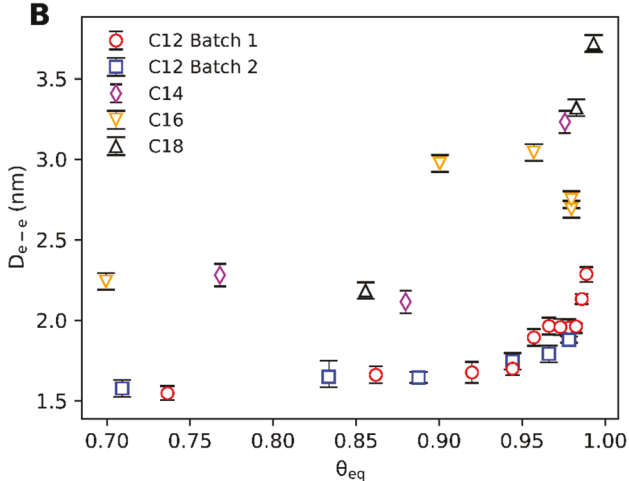
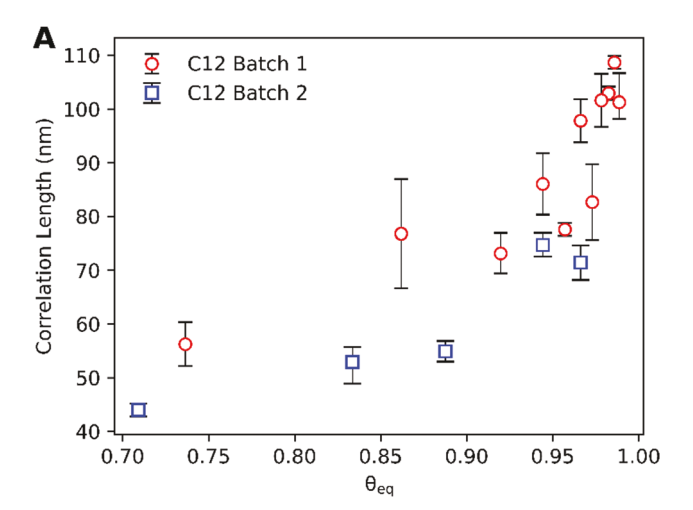


Fig. 3 (A) Increasing NP-NP edge-to-edge distance with increasing fractional surface coverage of dodecane thiol ligated Au nanoparticles. (B) Increasing NP-NP edge-to-edge distance with increasing fractional surface coverage of Au nanoparticles with thiols with chain lengths n = 12-18

Paper

function of  $\theta_{\rm eq}$  for samples of AuNPs ligated with tetradecanethiol, hexadecanethiol, and octadecanethiol, along with that of dodecanethiol ligated AuNPs for comparison. Note that the lengths of our fully extended thiol molecules,  $L_{\rm fe}$ , are 1.77 nm, 2.03 nm, 2.28 nm, and 2.54 nm, respectively, for dodecanethiol, tetradecanethiol, hexadecanethiol, and octadecanethiol;  $L_{\text{fe}}$  (nm) = 0.25 + 0.127n, where n is the number of CH2 groups, is determined by the empirical formula given by Bain et al. 18,33,40 Our GIXD results show that even as  $\theta_{eq}$ approaches 1, the edge-to-edge NP-NP separation is still less than 80% of twice that of  $L_{\rm fe}$ , indicating that the thiols are not fully extended between the AuNPs.

We also examined the correlation length,  $L_c$ , of the crystalline AuNP monolayers as a function of the surface coverage of the thiols on the Au cores as shown in Fig. 4A, where  $L_c$ is inversely proportional to the width of the first order Bragg peak (Fig. 4B) and proportional to the size of AuNP crystal domains.



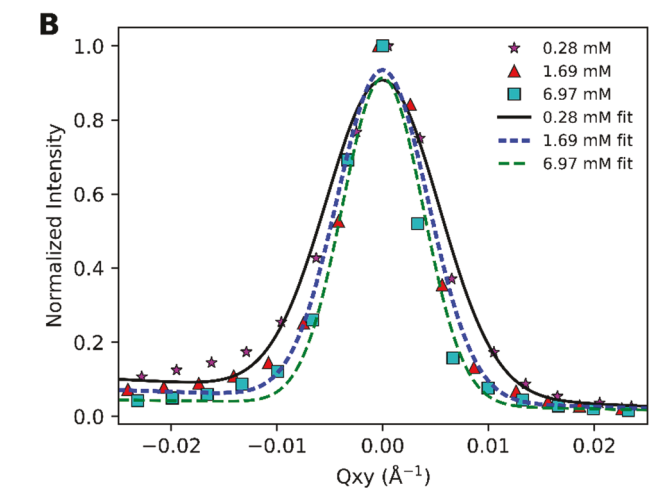


Fig. 4 (A) The correlation length as a function of surface coverage inferred from the widths of the first order diffraction peaks. (B) The shape of the first-order Bragg peaks of GIXD patterns for the NP monolayers examined in Fig. 2B. The raw data is fitted with a superposed Gaussian and inverse quadratic function, and subsequently normalized and translated such that the points are centered at the origin

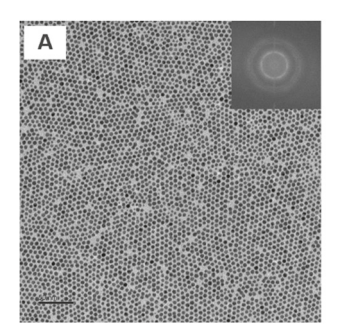
Liu, Lu and Zhai reported molecular dynamics simulations of the edge-to-edge NP-NP separation,  $D_{e-e}$ , in a three-dimensional nanocrystal of 2.83 nm Au cores ligated with hexane thiol, octane thiol and decane thiol as a function of surface coverage. 41 Their results show that all of these ligands generate the same rate of increase in  $D_{e-e}$  with surface coverage, namely 0.10-0.12 nm per 10% increase in thiol concentration. Molecular dynamics simulations of the potential of mean force between dodecanethiol ligated 5 nm Au cores carried out in this laboratory predict that the minimum in the potential of mean force increases 0.60 nm per 10% change in surface coverage. 42 Our data for  $D_{e-e}$  of the dodecane thiol capped Au cores of both batch #1 and batch #2 show, as a function of surface coverage, an increase of about 0.32 nm per 10% increase in thiol coverage (Fig. 3A). The increase in  $D_{e-e}$  with thiol surface coverage in these same samples was detected by Griesemer et al.35 from analysis of TEM images, but a quantitative relationship was not then established.

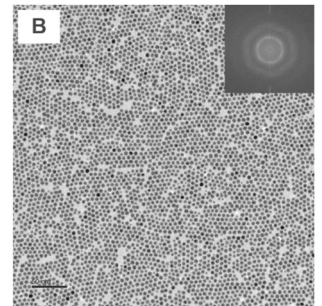
The simulations of the pair potential of mean force between dodecanethiol ligated Au cores reported by Liepold et al. 42 also show that even at 96% surface coverage the ligands are not quite fully extended, and that the ligands bend away from overlap at the equilibrium NP-NP separation. These calculations do not reveal the occurrence of crystal-like ordering of the ligands even at the highest surface coverage. They show that order along the ligand chain is lost after the first few C-C bonds at low ligand coverage (11%) and after about 8 C-C bonds at high ligand coverage (96%). The effective thickness of the calculated ligand envelope does increase with increased surface coverage and, therefore, it is reasonable to expect that the edgeto-edge NP-NP separation will increase with increasing ligand surface coverage and slowly approach an asymptotic value somewhat less than 3.54 nm for dodecanethiol depending on the extent of ligand bending and ligand shell interpenetration. As seen in Fig. 3, our GIXD data show that the edge-to-edge NP-NP separation increases slowly for surface coverage less than about 0.90, and very rapidly for larger surface coverage. In the systems we have studied we find that the edge-to-edge NP-NP separation never reaches the asymptotic value corresponding to non-penetrating fully extended ligand chains.

We find a similar trend upon examining TEM images of monolayers with the same thiol concentrations as used for the GIXD data displayed in Fig. 2B. We identify the irregular holes in these images to be the residues of thiol islands which increase in size as the thiol concentration increases (see Fig. 5A-C). Put another way, excess ligands aggregate in the space between NPs in the monolayer in the form of microdroplets, thereby contributing to isolation of ordered domains of fully ligated NPs without increasing the NP-NP separation.

Our GIXD data reveal an increase in the correlation length in the ordered domains of the NP monolayer as the thiol concentration increases (Fig. 4A). This result is consistent with the notion that the smaller the ligand fractional coverage the less uniform the ligand distribution on the Au core, likely leading to a less well-ordered NP solid. It is also consistent with segregation of the system into slightly larger excess lipid and ordered NP domains as the excess lipid concentration increases.

Soft Matter Paper





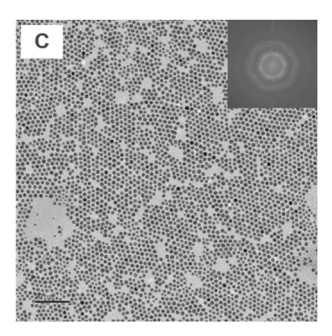


Fig. 5 TEM images of films formed from NP preparations with (A) 0.28, (B) 1.69, and (C) 6.97 mM of thiol concentrations in solution of dodecanethiol ligated AuNPs from sample batch 2. Two-dimensional Fourier transforms of TEM images are shown in the right-hand corner. Scale bars are 50 nm. An increase in thiol island size is evident with increasing thiol concentration.

## Conclusions

We have shown that under conventional conditions for their synthesis only partial coverage of Au cores with thiol ligands is generated. The rate of formation and the equilibrium coverage of AuNPs is adequately (but not perfectly) described by Langmuir adsorption kinetics. The consequences of partial coverage of the Au core are exhibited in the corresponding AuNP monolayer, specifically in the nanoparticle-nanoparticle interactions and long-range order in the monolayer. The clear gaps shown in the TEM images, which we suggest are holes that are the residues of islands of excess thiol in the monolayer, are consistent with GIXD measurements that reveal an increase in edge-to-edge spacing of the AuNPs. The GIXD data also reveal an increase in the correlation length in the monolayer with increasing excess thiol. The important observation used in this paper to describe packing effects in thiolated AuNP monolayers is that the free energy of binding of a thiol to an Au core implies that under usual conditions the surface of the Au core is partially covered by thiol molecules, and that the fractional coverage can be varied by changing the thiol concentration in the bulk. This important feature of the equilibrium between thiol concentration and surface coverage of the Au core has not been addressed previously.

### Conflicts of interest

There are no conflicts to declare.

# Acknowledgements

We thank Sophie Macfarland for intellectual discussions; Xiao-Min Lin for providing AuNPs samples and explaining the procedure for washing the AuNPs; and Dmitri Talapin for lending use of the ICP-OES. This research was primarily supported by the University of Chicago Materials Research Science and Engineering Center, funded by the National Science Foundation (Grant No. DMR-1420709), and partially supported by a Senior Mentor Grant from the Camille and Henry Dreyfus Foundation (Grant No. SI-14-014). NSF's ChemMatCARS Sector 15 is supported by the Divisions of Chemistry (CHE) and Materials Research (DMR), National Science Foundation, under grant number NSF/CHE-1834750. Use of the Advanced Photon Source, an Office of Science User Facility operated for the U.S. Department of Energy (DOE) Office of Science by Argonne National Laboratory, was supported by the U.S. DOE under Contract No. DE-AC02-06CH11357.

## References

- 1 A. L. González, C. Noguez and A. S. Barnard, J. Phys. Chem. C, 2012, **116**, 14170-14175.
- 2 A. Sánchez-Iglesias, M. Grzelczak, J. Pérez-Juste and L. M. Liz-Marzán, Angew. Chem., Int. Ed., 2010, 49, 9985-9989.
- 3 T. Franzl, T. Wilk, J. Feldmann, C. Sönnichsen and G. von Plessen, New J. Phys., 2002, 4, 93.
- 4 R. Parthasarathy, X.-M. Lin, K. Elteto, T. F. Rosenbaum and H. M. Jaeger, Phys. Rev. Lett., 2004, 92, 076801.
- 5 T. B. Tran, I. S. Beloborodov, X. M. Lin, T. P. Bigioni, V. M. Vinokur and H. M. Jaeger, Phys. Rev. Lett., 2005, 95, 076806.
- 6 C. T. Black, C. B. Murray, R. L. Sandstrom and S. Sun, Science, 2000, 290, 1131-1134.
- 7 C. Y. Lau, H. Duan, F. Wang, C. Bin He, H. Y. Low and J. K. W. Yang, Langmuir, 2011, 27, 3355-3360.
- 8 V. Santhanam, J. Liu, R. Agarwal and R. P. Andres, Langmuir, 2003, 19, 7881-7887.
- 9 J. He, P. Kanjanaboos, N. L. Frazer, A. Weis, X. M. Lin and H. M. Jaeger, Small, 2010, 6, 1449-1456.
- 10 Z. Nie, A. Petukhova and E. Kumacheva, Nat. Nanotechnol., 2010, 5, 15-25.
- 11 M. A. Dobrovolskaia and S. E. McNeil, Nat. Nanotechnol., 2007, 2, 469-478.
- 12 G. F. Paciotti, J. Zhao, S. Cao, P. J. Brodie, L. Tamarkin, M. Huhta, L. D. Myer, J. Friedman and D. G. I. Kingston, Bioconjugate Chem., 2016, 27, 2646-2657.
- 13 Z. Yuan, C. C. Hu, H. T. Chang and C. Lu, Analyst, 2016, 141,
- 14 L. Zhu, X. Shao, Y. Luo, K. Huang and W. Xu, ACS Chem. Biol., 2017, 12, 1373-1380.
- 15 E. Hutter and D. Maysinger, Trends Pharmacol. Sci., 2013, **34**, 497-507.
- 16 Z.-Y. Deng, K.-L. Chen and C.-H. Wu, Sci. Rep., 2019, 9, 1-8.

Paper Soft Matter

- 17 B. L. V. Prasad, S. I. Stoeva, C. M. Sorensen and K. J. Klabunde, Langmuir, 2002, 18, 7515-7520.
- 18 C. D. Bain, E. B. Troughton, Y.-T. Tao, J. Evall, G. M. Whitesides and R. G. Nuzzo, J. Am. Chem. Soc., 1989, 111, 321-335.
- 19 M. D. Porter, T. B. Bright, D. L. Allara and C. E. D. Chidsey, I. Am. Chem. Soc., 1987, 109, 3559-3568.
- 20 K. D. Comeau and M. V. Meli, Langmuir, 2012, 28, 377-381.
- 21 R. T. M. Jakobs, J. van Herrikhuyzen, J. C. Gielen, P. C. M. Christianen, S. C. J. Meskers and A. P. H. J. Schenning, J. Mater. Chem., 2008, 18, 3438-3441.
- 22 B. L. V. Prasad, C. M. Sorensen and K. J. Klabunde, Chem. Soc. Rev., 2008, 37, 1871-1883.
- 23 M. Benkovičová, A. Hološ, P. Nádaždy, Y. Halahovets, M. Kotlár, J. Kollár, P. Šiffalovič, M. Jergel, E. Majková, J. Mosnáček and J. Ivančo, Phys. Chem. Chem. Phys., 2019, 21, 9553-9563.
- 24 K. J. Si, Y. Chen, Q. Shi and W. Cheng, Adv. Sci., 2018, 5, 1700179.
- 25 F. Schreiber, Prog. Surf. Sci., 2000, 65, 151-256.
- 26 E. Pensa, E. Cortés, G. Corthey, P. Carro, C. Vericat, M. H. Fonticelli, G. Benítez, A. A. Rubert and R. C. Salvarezza, Acc. Chem. Res., 2012, 45, 1183-1192.
- 27 A. N. Bordenyuk, C. Weeraman, A. Yatawara, H. D. Jayathilake, I. Stiopkin, Y. Liu and A. V. Benderskii, J. Phys. Chem. C, 2007, 111, 8925-8933.
- 28 W. Pan, C. J. Durning and N. J. Turro, Langmuir, 1996, 12, 4469-4473.
- 29 R. Desikan, I. Lee and T. Thundat, *Ultramicroscopy*, 2006, 106, 795-799.

- 30 A. Kassam, G. Bremner, B. Clark, G. Ulibarri and R. B. Lennox, I. Am. Chem. Soc., 2006, 128, 3476-3477.
- 31 D. S. Karpovich and G. J. Blanchard, Langmuir, 1994, 10, 3315-3322.
- 32 S. M. Ansar, F. S. Mohammed, G. Von White, M. Budi, K. C. Powell, O. T. Mefford and C. L. Kitchens, J. Phys. Chem. C, 2016, 120, 6842-6850.
- 33 C. D. Bain, J. Evall and G. M. Whitesides, J. Am. Chem. Soc., 1989, 111, 7155-7164.
- 34 H. Cheng, L. Yang, Y. Jiang, Y. Huang, Z. Sun, J. Zhang, T. Hu, Z. Pan, G. Pan, T. Yao, Q. Bian and S. Wei, Nanoscale, 2013, 5, 11795-11800.
- 35 S. D. Griesemer, S. S. You, P. Kanjanaboos, M. Calabro, H. M. Jaeger, S. A. Rice and B. Lin, Soft Matter, 2017, 13, 3125-3133.
- 36 X.-M. Lin, C. M. Sorensen and K. J. Klabunde, J. Nanopart. Res., 2000, 2, 157-164.
- 37 Z. Jiang, J. He, S. A. Deshmukh, P. Kanjanaboos, G. Kamath, Y. Wang, S. K. R. S. Sankaranarayanan, J. Wang, H. M. Jaeger and X. M. Lin, Nat. Mater., 2015, 14, 912-917.
- 38 D. G. Schultz, X. M. Lin, D. Li, J. Gebhardt, M. Meron, P. J. Viccaro and B. Lin, J. Phys. Chem. B, 2006, 110, 24522-24529.
- 39 I. Kosif, K. Kratz, S. S. You, M. K. Bera, K. Kim, B. Leahy, T. Emrick, K. Y. C. Lee and B. Lin, ACS Nano, 2017, 11, 1292-1300.
- 40 L. Motte and M. P. Pileni, J. Phys. Chem. B, 1998, 102, 4104-4109.
- 41 X. Liu, P. Lu and H. Zhai, J. Chem. Phys., 2019, 150, 034702.
- 42 C. Liepold, A. Smith, B. Lin, J. de Pablo and S. A. Rice, J. Chem. Phys., 2019, 150, 044904.